ACS Chemical Neuroscience

pubs.acs.org/chemneuro

Research Article

Characterization of a Conformation-Restricted Amyloid β Peptide and Immunoreactivity of Its Antibody in Human AD brain

Yusuke Kageyama, Yumi Irie, Yuka Matsushima, Tatsuya Segawa, Jean-Pierre Bellier, Kumi Hidaka, Hiroshi Sugiyama, Daita Kaneda, Yoshio Hashizume, Hiroyasu Akatsu, Kunio Miki, Akiko Kita, Douglas G. Walker, Kazuhiro Irie, and Ikuo Tooyama*

Cite This: *ACS Chem. Neurosci.* 2021, 12, 3418−3432

Read Online

ACCESS | Metrics & More | Article Recommendations

ABSTRACT: Characterization of amyloid β (Aβ) oligomers, the transition species present prior to the formation of Aβ fibrils and that have cytotoxicity, has become one of the major topics in the investigations of Alzheimer's disease (AD) pathogenesis. However, studying pathophysiological properties of Aβ oligomers is challenging due to the instability of these protein complexes *in vitro*. Here, we report that conformation-restricted Aβ42 with an intramolecular disulfide bond at positions 17 and 28 (SS-Aβ42) formed stable Aβ oligomers *in vitro*. Thioflavin T binding assays, nondenaturing gel electrophoresis, and morphological analyses revealed that SS-Aβ42 maintained oligomeric structure, whereas wild-type Aβ42 and the highly aggregative Aβ42 mutant with E22P substitution (E22P-Aβ42) formed Aβ fibrils. In agreement with these observations, SS-Aβ42 was more cytotoxic compared to the wild-type and E22P-Aβ42 in cell cultures. Furthermore, we developed a monoclonal antibody, designated TxCo-1, using the toxic conformation of SS-Aβ42 as immunogen. X-ray crystallography of the TxCo-1/SS-Aβ42 complex, enzyme immunoassay, and immunohistochemical studies confirmed the recognition site and specificity of TxCo-1 to SS-Aβ42. Immunohistochemistry with TxCo-1 antibody identified structures resembling senile plaques and vascular Aβ in brain samples of AD subjects. However, TxCo-1 immunoreactivity did not colocalize extensively with Aβ plaques identified with conventional Aβ antibodies. Together, these findings indicate that Aβ with a turn at positions 22 and 23, which is prone to form Aβ oligomers, could show strong cytotoxicity and accumulated in brains of AD subjects. The SS-Aβ42 and TxCo-1 antibody should facilitate understanding of the pathological role of Aβ with toxic conformation in AD.

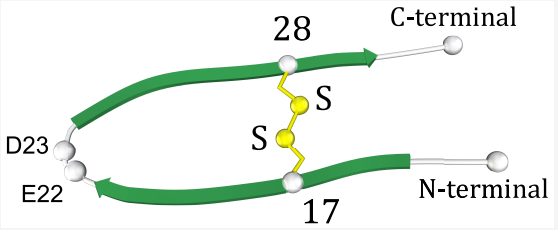

KEYWORDS: *THP-1, Aβ oligomer, protofibril, Aβ fibril, Aβ toxic conformer, Alzheimer's disease*

INTRODUCTION

Amyloid β (Aβ) plays a critical role in the pathogenesis of Alzheimer's disease (AD).[1,2] Aberrant accumulation of Aβ leads to formation of Aβ plaques and subsequent neurodegeneration.[3] Aβ plaques consist of highly ordered fibrillar aggregates of Aβ. The formation of Aβ fibrils takes several steps: oligomerization of monomeric Aβ, formation of protofibrils from Aβ oligomers, and aggregation into Aβ fibrils.[4,5] Studies have shown that Aβ oligomers, an intermediate transition form of Aβ, have more neurotoxic effects compared with Aβ fibrils.[6−8] Many factors could influence formation of toxic Aβ oligomers. Cellular membranes appear to play an important role in promoting formation of Aβ oligomers.[9] Aβ fibrils can bind to monosialotetrahexosylganglioside (GM1) in rafts with various membrane-bound conformations that cause membrane disruption.[10−12] Metal ions like copper and zinc are also involved in the aggregation process of Aβ.[9] Although Aβ42 is more neurotoxic than Aβ40 as a single alloform, the interplay between these Aβ species might also be important in AD pathology.[13] Computer simulations predicted the structure of disordered Aβ in solution.[14] Further detailed studies of Aβ oligomers are warranted, yet are challenging due to the instability of these protein complexes *in vitro*.

Cross-linkage of Aβ is one strategy to investigate Aβ oligomers.[15−17] The tertiary structure of Aβ oligomers can be fixed either by inducing cross-linking of the proteins with amino acid substitutions or by using a cross-linking reagent. Formation of an intramolecular bond is a different strategy to stabilize Aβ oligomers.[18] Sandberg et al. generated Aβ42 with an intramolecular disulfide bond at positions 21 and 30 (Aβcc) and showed that it formed stable oligomers and was resistant

Received: June 23, 2021
Accepted: August 10, 2021
Published: August 31, 2021

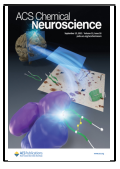

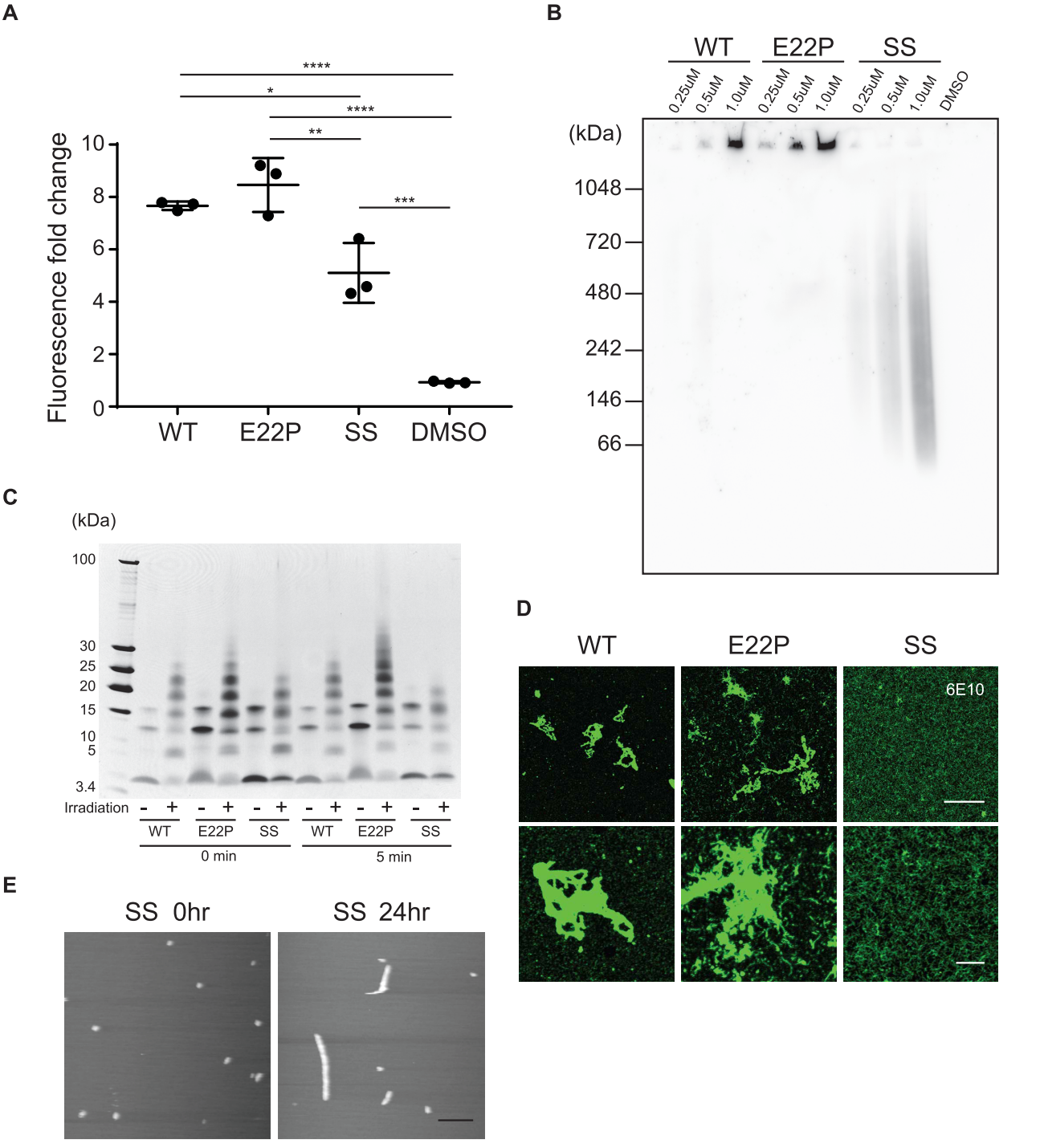

Figure 1. Features of fibrillization of WT-Aβ42, E22P-Aβ42, SS-Aβ42 in PBS. (A) Fibrillization of Aβ peptides in PBS was assessed by Th-T binding assay. Fluorescence fold change indicates that E22P-Aβ42 and WT-Aβ42 showed high trend of Aβ fibrillization, followed by SS-Aβ42. Values are average ± SD (n = 3). (B) The size and nature of Aβ aggregates were assessed by nondenaturing PAGE. WT-Aβ42 and E22P-Aβ42 showed protein bands at the size over 1000 kDa, while SS-Aβ42 exhibited a variable smear. (C) WT-Aβ42, E22P-Aβ42, and SS-Aβ42 were cross-linked using PICUP. The 0 min samples were subjected to PICUP immediately after being dissolved in phosphate buffer. The 5 min samples were incubated at 37 °C for 5 min prior to PICUP. The samples were analyzed by tricine−SDS/PAGE and visualized by silver staining. The band patterns of WT-Aβ42 and SS-Aβ42 showed little difference, whereas a 5 min incubation promoted the rapid Aβ oligomerization of E22P-Aβ42. (D) Morphology of Aβ aggregates formed in PBS and attached on cover glass was observed by confocal microscopy. Top row shows representative images taken by ×63 objective lens, and bottom row shows images taken by ×63 objective lens with ×3 zoom. WT-Aβ42 and E22P-Aβ42 became fibrils in size over 20 μm. Thread-like Aβ appeared all over the field in E22P-Aβ42. Countless bead-like structures attached on the surface of cover glass with SS-Aβ42. Scale bar, 20 μm in top row and 5 μm in bottom row. (E) Morphology of the protein complexes of SS-Aβ42 formed in PBS was observed by atomic force microscopy. Left panel shows the morphology of SS-Aβ42 prior to the incubation, and right panel shows its morphology after 24 h incubation. Size, around 50 nm, and morphology of SS-Aβ42 were uniform prior to the incubation. After the incubation, some of the SS-Aβ42 extended their size up to 400 nm, and others remained the same size. Scale bar, 200 nm. Data information: Significance was calculated using one-way ANOVA with post hoc Tukey: *P < 0.05, **P < 0.01, ***P < 0.001, ****P < 0.0001.

https://doi.org/10.1021/acschemneuro.1c00416
ACS Chem. Neurosci. 2021, 12, 3418−3432

to forming fibrils. This study suggested that the conformational locking of monomeric Aβ partially inhibits the formation of intermolecular hydrogen bonds between β-strands of Aβ, thereby stabilizing Aβ complexes as oligomers.

Analysis of aggregates of Aβ42 with systematic proline replacement followed by solid-state nuclear magnetic resonance (NMR) revealed that Aβ42 adopts two conformations: one with a turn at positions 22 and 23, another with a turn at positions 25 and 26.[19−22] These studies revealed that Aβ42 with a turn at positions 22 and 23 was highly aggregative and neurotoxic.[23] For intrinsically disordered proteins like Aβ, structural perturbation by chiral inversion of the focused amino acid residue (chiral editing) could be valuable to investigate their conformational change.[24] Substitution of L-Glu with D-Glu at position 22 of Aβ42 attenuated propensity to form fibrils and enhanced cytotoxicity against PC12 cells.[25] Age-related epimerization at Ser26 reduced the toxicity of Aβ42 by stabilization of the aggregation intermediates.[26] Systematic chiral mutation at the central region of Aβ42 revealed that D-amino acid replacement at Glu22 makes Aβ42 more soluble and more neurotoxic, while that at Ser26 makes Aβ42 even more soluble but non-neurotoxic.[27,28] These data are in agreement with our hypothesis of the existence of a toxic conformer with a turn at positions 22 and 23 and that of the less toxic conformer with a turn at positions 25 and 26.[22,23] Matsushima et al. developed a conformation-restricted Aβ42 with an intramolecular disulfide bond at positions 17 and 28 (SS-Aβ42) to stabilize the toxic turn at positions 22 and 23 without proline replacement.[29] This synthetic form of Aβ42 displayed stronger neurotoxicity against SH-SY5Y cells and more resistance to the formation of Aβ fibrils compared to the wild-type Aβ42 (WT-Aβ42). This is the first example of conformation-restricted toxic Aβ42 with wild-type sequence from position 19 to position 26. This result could be due to the stabilization of Aβ oligomers by conformational lock at positions 17 and 28 via disulfide bond which consecutively could stabilize the toxic turn at positions 22 and 23 and inhibits partially the formation of intermolecular parallel β-strands of Aβ42, a crucial stage in Aβ fibrillization.

The purpose of this study was to further investigate SS-Aβ42 in the context of Aβ fibrillization and cytotoxicity compared to WT-Aβ42 and the highly aggregative Aβ42 mutant with E22P substitution (E22P-Aβ42), thereby to establish it as a tool to study Aβ oligomers *in vitro*. Furthermore, we generated a monoclonal antibody, designated TxCo-1, using SS-Aβ42 as immunogen to study toxic Aβ oligomers in brain tissue. Since SS-Aβ42 retains native peptide sequence from position 19 to position 26, the antibody TxCo-1 targeting the toxic turn could be an ideal tool to study the presence of toxic forms of Aβ in brain tissue.

RESULTS AND DISCUSSION

Fibrillization of Aβ Peptides in PBS. Features of fibrillization of Aβ peptides in PBS were assessed by thioflavin T (Th-T) binding assay, nondenaturing PAGE, and morphological analysis. 4 μM WT-Aβ42, E22P-Aβ42, and SS-Aβ42 peptides were incubated in PBS for 24 h at 37 °C. The samples were mixed with Th-T, adjusting its concentration at 20 μM, and then further incubated for 12 h at 24 °C. Then, fluorescence intensity was measured (Figure 1A). On the basis of the fluorescence fold changes, WT-Aβ42 and E22P-Aβ42 showed the highest trend of Aβ fibrillization, followed by SS-Aβ42. Next, we confirmed the molecular size of Aβ aggregates formed in PBS. 0.25, 0.5, and 1.0 μM WT-Aβ42, E22P-Aβ42, and SS-Aβ42 peptides were incubated in PBS for 24 h at 37 °C, and the size of Aβ aggregates was assessed under nondenaturing conditions by blue-native gel electrophoresis (Figure 1B). A single band of over 1000 kDa appeared at the top of the lanes in WT-Aβ42 and E22P-Aβ42, and the signal intensity increased with increasing concentrations of the Aβ peptides. In contrast, SS-Aβ42 showed smears ranging roughly from 50 to 1000 kDa, and the signal intensity increased with increasing concentration of the Aβ peptide. These data indicate that WT-Aβ42 and E22P-Aβ42 become aggregates with sizes over 1000 kDa in PBS, while SS-Aβ42 formed different types of aggregates of various sizes less than 700 kDa (150-mer). Next, in order to assess the rate of Aβ aggregation, we prepared Aβ oligomers and stabilized the structure by cross-linking with photo-induced cross-linking of unmodified proteins (PICUP).[15] PICUP is a method that enables formation of covalent bonds between closely interacting polypeptides such as Aβ oligomers to monitor the formation of the protein complexes. 50 μM WT-Aβ42, E22P-Aβ42, and SS-Aβ42 peptides were used immediately in PICUP assay (0 min) after being dissolved in phosphate buffer or were incubated at 37 °C for 5 min prior to the experiment. The band patterns of WT-Aβ42 and SS-Aβ42 showed little difference, whereas a 5 min incubation promoted the rapid Aβ oligomerization of E22P-Aβ42. These data suggest that the rate of Aβ42 oligomerization is faster in E22P-Aβ42. Lastly, we observed the morphology of Aβ aggregates formed in PBS. 1.0 μM WT-Aβ42, E22P-Aβ42, SS-Aβ42 peptides were incubated in PBS for 24 h at 37 °C and observed by confocal microscopy (Figure 1D). WT-Aβ42 and E22P-Aβ42 peptides formed structures resembling typical Aβ fibrils with sizes over 20 μm. In E22P-Aβ42, rope and bead-like Aβ appeared uniformly in the observed fields. In contrast, large Aβ aggregates were not observed in SS-Aβ42, and numerous fine thread and bead-like structures smaller than those observed in E22P-Aβ42 appeared uniformly in the observed field. Since the morphology of aggregates formed by SS-Aβ42 was not well-defined by confocal microscopy, we examined it in further detail by atomic force microscopy (AFM) (Figure 1E). SS-Aβ42 displayed uniform shape and size prior to the incubation. With 24 h incubation, some SS-Aβ42 formed aggregates. On the basis of results of low Th-T binding and gel migration pattern, we suggest that SS-Aβ42 does not form structures resembling typical Aβ fibrils in PBS and remains as oligomers of various sizes.

The degree of Aβ oligomerization/fibrillization of SS-Aβ42 was monitored by Th-T binding assay, nondenaturing PAGE, PICUP, and morphological analyses comparing the results with those of WT-Aβ42 and E22P-Aβ42. We found that SS-Aβ42 did not form the large fibrils observed in WT-Aβ42 and E22P-Aβ42 and remained as small particles resembling protofibril in PBS. The result of PICUP experiment suggests that E22P-Aβ42 has a faster rate of oligomerization. However, caution should be made in the interpretation of the PICUP data. In our hands, identification of oligomers higher than heptamers might be difficult to detect by PICUP.[15,30] However, Aβ42 aggregates of higher molecular weight were observed using nondenaturing PAGE. The results of PICUP and nondenaturing PAGE indicate that SS-Aβ42 does not form the Aβ fibrils observed in WT-Aβ42 and E22P-Aβ42.

Fibrillization of Aβ Peptides in Cell Culture Media. To investigate fibrillization of Aβ peptides in solution with

https://doi.org/10.1021/acschemneuro.1c00416
ACS Chem. Neurosci. 2021, 12, 3418−3432

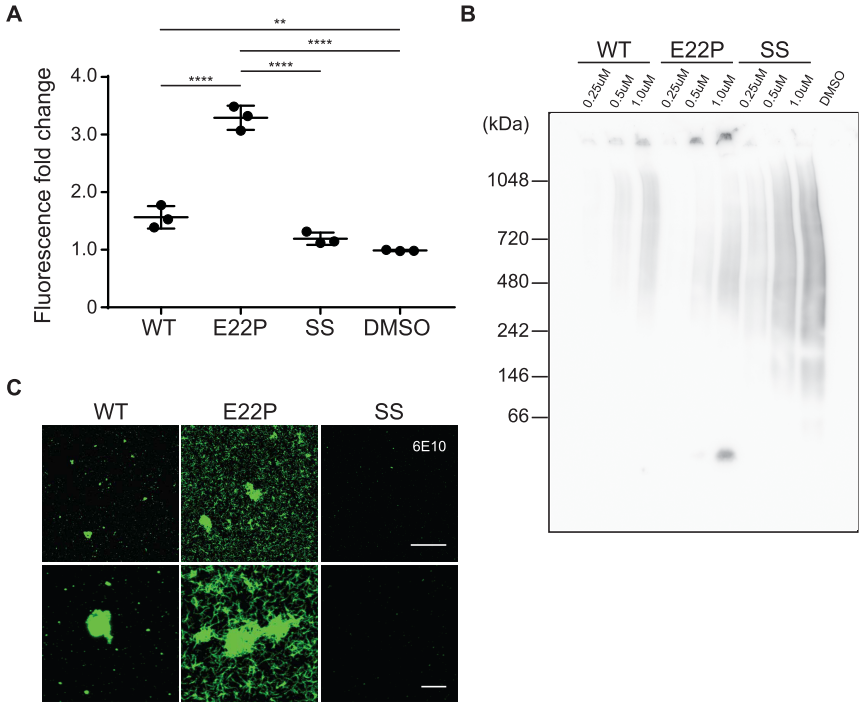

Figure 2. Features of fibrillization of WT-Aβ42, E22P-Aβ42, SS-Aβ42 in cell culture media. (A) Fibrillization of Aβ peptides in 1% FBS/RPMI1640 was assessed by Th-T binding assay. E22P-Aβ42 showed high trend of Aβ fibrillization compared to WT-Aβ42 and SS-Aβ42. Values are average ± SD (n = 3). (B) The size of Aβ aggregates was assessed by nondenaturing PAGE. WT-Aβ42 and E22P-Aβ42 showed both protein bands at the size over 1000 kDa and smear ranging from 200 to over 1000 kDa, while SS-Aβ42 exhibited smear. (C) Morphology of Aβ aggregates formed in 1% FBS/RPMI1640 and attached on the cover glass was observed by confocal microscopy. Top row shows representative images taken by ×63 objective lens, and bottom row show images taken by ×63 objective lens with ×3 zoom. Size of fibril in WT-Aβ42 reduced to 1−5 μm. Size of fibril in E22P-Aβ42 reduced to <10 μm, while thread-like Aβ remained similar. Noticeable Aβ was not observed in SS-Aβ42 suggesting it remained in soluble form. Scale bar, 20 μm in top row and 5 μm in bottom row. Data information: Significance was calculated using one-way ANOVA with post hoc Tukey: $^{**}P < 0.01$, $^{****}P < 0.0001$.

complex biological constituents, we conducted Th-T binding assays, nondenaturing PAGE, and morphological analysis on Aβ peptides incubated in 1% FBS/RPMI1640 culture media. 4 μM WT-Aβ42, E22P-Aβ42, and SS-Aβ42 peptides were incubated in 1% FBS/RPMI1640 for 24 h at 37 °C. The samples were mixed with Th-T, adjusting its concentration to 20 μM, and further incubated for 12 h at 24 °C. Then, fluorescence intensity was measured (Figure 2A). On the basis of the fluorescence fold changes, E22P-Aβ42 showed the high trend of Aβ fibrillization compared to WT-Aβ42 and SS-Aβ42. Next, we assessed the size of Aβ oligomers formed in 1% FBS/RPMI1640. 0.25, 0.5, and 1.0 μM WT-Aβ42, E22P-Aβ42, SS-Aβ42 peptides were incubated in 1% FBS/RPMI1640 for 24 h at 37 °C, and the size of aggregates was assessed under nondenaturing conditions by blue-native gel electrophoresis (Figure 2B). For WT-Aβ42 and E22P-Aβ42, a single band over 1000 kDa appeared at the top of the lane together with smears ranging from roughly 200 to over 1000 kDa. The signal intensity increased with concentration of these Aβ peptides. In the lane loaded with E22P-Aβ42 at 1.0 μM, a band appeared below the molecular marker at 66 kDa. In contrast, SS-Aβ42 showed a smear ranging roughly from 50 to over 1000 kDa. Lastly, we observed morphology of Aβ aggregates formed in 1%FBS/RPMI1640. 1.0 μM WT-Aβ42, E22P-Aβ42, SS-Aβ42 peptides were incubated in 1% FBS/RPMI1640 for 24 h at 37 °C and observed by confocal microscopy (Figure 2C). WT-Aβ42 and E22P-Aβ42 peptides formed a structure resembling Aβ fibrils/aggregates, yet its size was reduced to 10 μm or less. Rope-like Aβ aggregates appeared uniformly in E22P-Aβ42. In SS-Aβ42, noticeable Aβ signal could not be detected in the observed field. These results show the same trends as aggregation occurring in PBS, but the protein present in 1% FBS has significantly slowed down the complete aggregation of WT-Aβ42 and E22P-Aβ42.

The amount of Aβ fibrillization diminished in culture media with complex constituents. Plasma proteins, especially serum albumin, can be potent inhibitors of Aβ fibrillization.[31,32] The difference in results obtained with PBS and 1% FBS/RPMI media implies that Aβ polymerization is affected by the composition of the solution. Clearance of Aβ from brain parenchyma can be by multiple pathways, i.e., protein degradation, CSF, and bloodstream.[33,34] A future study correlating type of solvents and structure of Aβ complexes *in vivo* could help to understand the physiology of Aβ clearance.

Toxicity, Cellular Localization, and Uptake Dynamics of Aβ Peptides. A previous study confirmed higher neurotoxicity of E22P-Aβ42 and SS-Aβ42 compared to the WT-Aβ42 using the human neuroblastoma SH-SY5 cell line,[29] which is generally used as a model of neurons.[27,28] In the present study, we employed THP-1 macrophage-like cells to further explore the toxicity of these Aβ peptides. THP-1 is a human leukemia cell line, which has many properties of native monocyte-derived macrophage upon differentiation with phorbol ester.[35] It is an established cellular model of microglia for studying responses to Aβ properties.[36] Studies suggest microglia are major players in neuroinflammation for the pathogenesis of AD.[37,38] Differentiated THP-1 cells were incubated with WT-Aβ42, E22P-Aβ42, and SS-Aβ42 peptides

https://doi.org/10.1021/acschemneuro.1c00416
ACS Chem. Neurosci. 2021, 12, 3418−3432

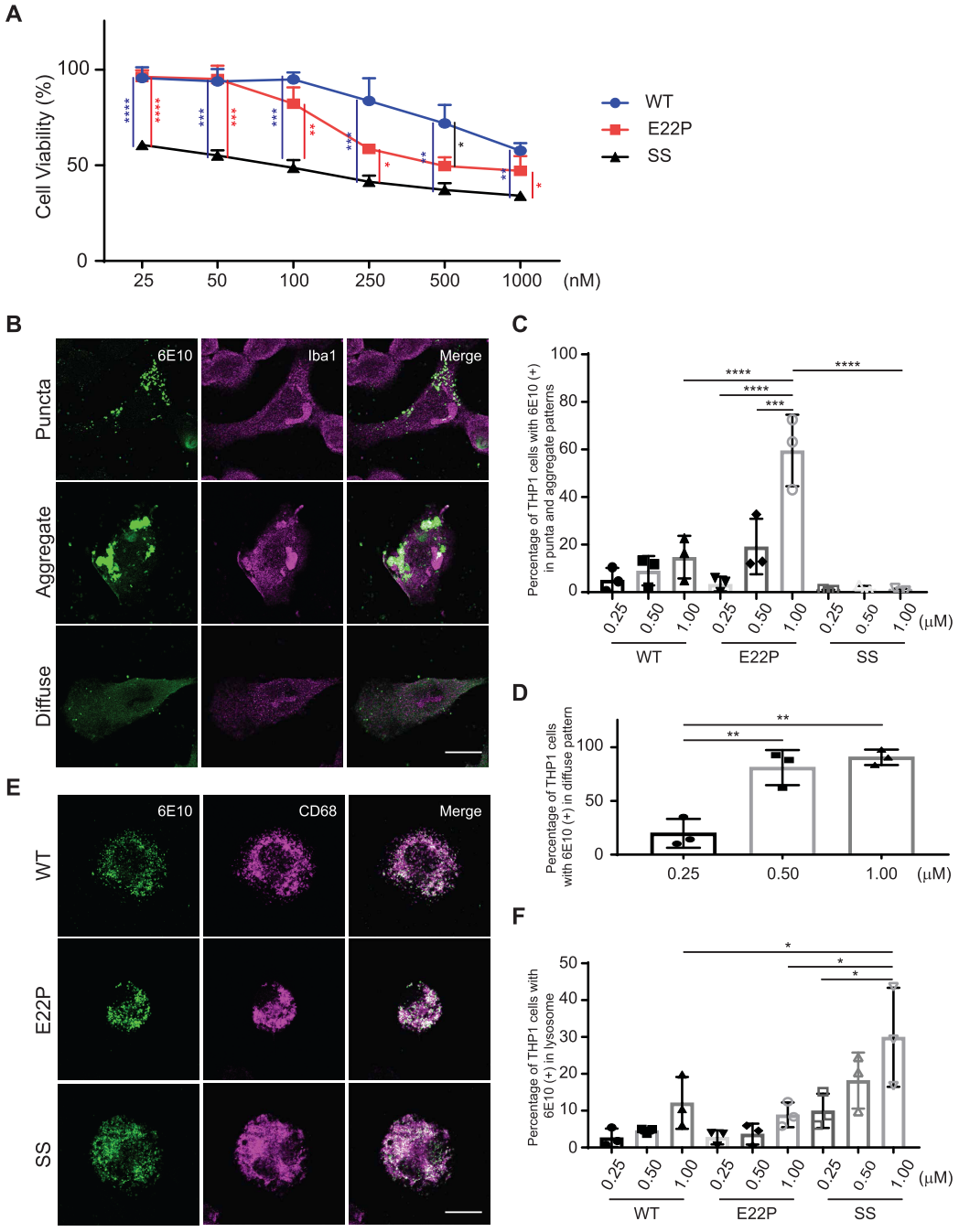

Figure 3. Toxicity, cellular localization, and uptake dynamics of Aβ peptides with THP1 cells. (A) Cytotoxicity of WT-Aβ42, E22P-Aβ42, and SS-Aβ42 was assessed by MTT assay. Values are average ± SD (n = 3 experiments). Statistical comparisons are indicated in blue for WT-Aβ42 and SS-Aβ42, red for E22P-Aβ42 and SS-Aβ42, and black for WT-Aβ42 and E22P-Aβ42. (B) Patterns of Aβ localization in THP1 cells. The representative images were taken with 63× objective lens. Scale bar, 20 μm. (C) Percentage of THP1 cells that showed localization pattern in puncta and aggregate category. Values are average ± SD (n = 3 experiments). (D) Percentage of THP1 cells treated with SS-Aβ42 and that showed localization pattern in diffuse category. Values are average ± SD (n = 3 experiments). (E) Colocalization of Aβ peptides with lysosome in THP1 cell upon treatment with bafilomycin A1. The representative images were taken with 63× objective lens. Scale bar, 20 μm. (F) Percentage of THP1 cells treated with bafilomycin A1 and that showed colocalization of 6E10 signal in lysosome. Values are average ± SD (n = 3 experiments). Data information: Significance was calculated using one-way ANOVA with post hoc Tukey in (A) and (D) and two-way ANOVA with post hoc Tukey in (C) and (F): *P < 0.05, **P < 0.01, ***P < 0.001, ****P < 0.0001.

at various concentrations in 1% FBS/RPMI1640 for 24 h at 37 °C, and cell viability was measured by MTT assay (Figure 3A). SS-Aβ42 showed cytotoxicity at quite low concentrations even at 25 nM, whereas WT-Aβ42 and E22P-Aβ42 exhibited a weaker effect though E22P-Aβ42 was more potent than WT-Aβ42 as previously reported in PC12 cells.[19,39] Next, we assessed the localization of these Aβ peptides in THP-1 cells upon treatment as a measure of cellular uptake and processing of these peptides. These Aβ peptides in THP-1 cells showed three different localization patterns: puncta, aggregate, and diffuse (Figure 3B). The THP1 cells in category puncta exhibited multiple dots of less than 1 μm. The size of 6E10

https://doi.org/10.1021/acschemneuro.1c00416
ACS Chem. Neurosci. 2021, 12, 3418−3432

signals in category aggregate was over 3 μm. In the diffuse pattern, the 6E10 signal was observed throughout the cell body. We quantified the fraction of THP1 cells that showed either puncta, aggregate, or both (Figure 3C). The fraction of THP1 cells in these categories increased in both WT-Aβ42 and E22P-Aβ42 as the concentration of these peptides increased, and E22P-Aβ42 showed more drastic change. In contrast, only around 1% of the cells exhibited these patterns upon SS-Aβ42 treatment. Rather, localization of SS-Aβ42 took a diffuse pattern, which was not evident in the cells treated with WT-Aβ42 and E22P-Aβ42. Over 80% of THP1 cells treated with SS-Aβ42 showed a diffuse pattern at 0.5 and 1.0 μM (Figure 3D). These data indicated that these Aβ peptides show different localization patterns in THP1 cells, while WT-Aβ42 and E22P-Aβ42 show similar patterns upon treatment. To test whether accumulation of these Aβ peptides and different localization patterns were due to the result of Aβ incorporation into the cells or attachment of these peptides to the surface of the cell membrane, we examined the accumulation of these Aβ peptides in the presence of bafilomycin A1, an inhibitor of lysosomal H^+-ATPases that blocks lysosomal degradation.[40] We found that these Aβ peptides colocalized with lysosomal marker CD68 (Figure 3E). Next, we quantified the fraction of THP1 cells labeled with both 6E10 and CD68 (Figure 3F). The fraction of dual labeled THP1 cells increased after treatment with WT-Aβ42 and E22P-Aβ42 as the concentration of these Aβ peptides increased, and SS-Aβ42 showed greater changes. These data indicate that THP1 cells are able to incorporate these Aβ peptides, but cells treated with SS-Aβ42 showed markedly increased dynamics.

Cytotoxicity of Aβ oligomers to various brain cells has been evaluated experimentally, and much research has affirmed their contribution to exacerbating AD pathology.[6,8,41] As expected, SS-Aβ42 displayed higher cytotoxicity on THP1 cells compared to WT-Aβ42 and E22P-Aβ42. However, a question remains as to what type of Aβ species causes this cytotoxicity since Aβ species in a variety of sizes formed in 1% FBS/RPMI. Previous findings suggest the difference in toxicity between high (above 50 kDa) and low molecular weight Aβ oligomers.[41] High molecular weight Aβ oligomers are implicated in inducing the formation of reactive oxygen species and lipid peroxidation, resulting in impairment of membrane integrity and subsequent LTP loss.[42] As a limitation of this study, we were not able to induce formation of Aβ aggregates of defined sizes and structures. To further dissect the pathophysiological role of Aβ species in different structures, development of methods for induction and purification of aggregates of constant size with potent neurotoxicity are needed. Dimerization of SS-Aβ42 at the C-terminal region might address this problem.[43]

Detection of an Epitope of SS-Aβ42 Antibody on Human Brain Tissue. To study specific conformation of SS-Aβ42, we produced a monoclonal antibody (TxCo-1) using SS-Aβ42 as an immunogen and characterized its immunoreactivity by X-ray crystallography, enzyme immunoassay, and immunohistochemistry.

After extensive screening, we obtained crystals diffracting to 2.5 Å resolution and its structure (Table 1). The SS-Aβ42 (15−30) peptide binds to the molecular surface of the TxCo-1 antibody (Figure 4). The residues 16−28 of SS-Aβ42 (15−30) are clearly observed in electron densities. Several interactions between SS-Aβ42 (15−30) and TxCo-1 are observed as indicated in Figure 4B. In addition to such interatomic interaction, there exist the $\pi-\pi$ stacking interaction between Phe19 in SS-Aβ42 (15−30) and Tyr103 of the H chain of TxCo-1 and the CH/π interaction between Phe20 in SS-Aβ42 (15−30) and Pro100 of L chain of TxCo-1. The crystal structure shows that TxCo-1 Fab recognizes the region including positions 22 and 23 of the truncated form of SS-Aβ42 (15−30), indicating that TxCo-1 is an antibody to the toxic turn structure of Aβ (Figure 4A,B). Specificity of the TxCo-1 antibody against SS-Aβ42 compared to WT-Aβ42 and E22P-Aβ42 was assessed with enzyme immunoassay. The TxCo-1 antibody showed high binding affinity against SS-Aβ42 (Figure 5A) but no significant immunoreactivity against WT-Aβ42 and E22P-Aβ42. Next, we optimized the conditions for immunohistochemistry with the TxCo-1 antibody on human brain tissue. Immunoreactivity with TxCo-1 antibody was detected in brain tissue from AD subjects upon pretreatment with formic acid and antigen retrieval with EDTA (Figure 5B). The TxCo-1 antibody-stained structures resembled neuritic and diffuse plaques (arrow) and vascular Aβ (arrowhead). To further confirm the specificity of the TxCo-1 antibody against SS-Aβ42, preabsorption tests were performed. Preincubation of the TxCo-1 antibody with its immunogen in 20-molar excess for 1 h at 37 °C abolished the TxCo-1 staining of senile plaques and blood vessels (Figure 5C). Furthermore, we assessed cross-reactivity of the TxCo-1 antibody against WT-Aβ42 and E22P-Aβ42. Preincubation of the TxCo-1 antibody

Table 1. Data Collection and Refinement

Data Collection Statistics	
protein	TxCo-1-SS-Aβ42 (15−30)
PDB code	7E6P
wavelength	1.000
space group	*C*2
cell dimensions	
a (Å)	185.0
b (Å)	40.5
c (Å)	69.4
β (deg)	97.2
no. of molecules per asymmetric unit	1
resolution (Å)	2.5
measurements	122,871
unique reflections	18065
R_{merge} [a]	0.091 (0.375) [b]
multiplicity	6.8 (6.9)
$I/\sigma(I)$	17.0 (5.3)
completeness (%)	100.0 (100.0)
overall *B* factor from Wilson plot (Å^2)	23.2
Refinement Statistics	
resolution (Å)	2.5
no. of reflections	17192
R_{work}/R_{free} [c,d] (%)	0.191/0.244
no. of atoms, Fab/peptide/others	3334/102/116
average *B* factor, Fab/peptide/others (Å^2)	31.1/38.0/32.8
rmsd from ideal geometry	
bond length (Å)	0.0034
bond angle (deg)	1.277
Ramachandran plot	
favored/outliers (%)	95.9/0.0

[a] $R_{merge} = \Sigma(|I - \langle I\rangle|)/\Sigma(I)$. [b] Numbers in parentheses refer to the highest-resolution shell, 2.55−2.5 Å. [c] $R = \Sigma||F_{obs}| - |F_{calc}||/\Sigma|F_{obs}|$. [d] R_{work} is calculated from a set of reflections in which 5% of the total reflections have been randomly omitted from the refinement and used to calculate R_{free}.

https://doi.org/10.1021/acschemneuro.1c00416
ACS Chem. Neurosci. 2021, 12, 3418−3432

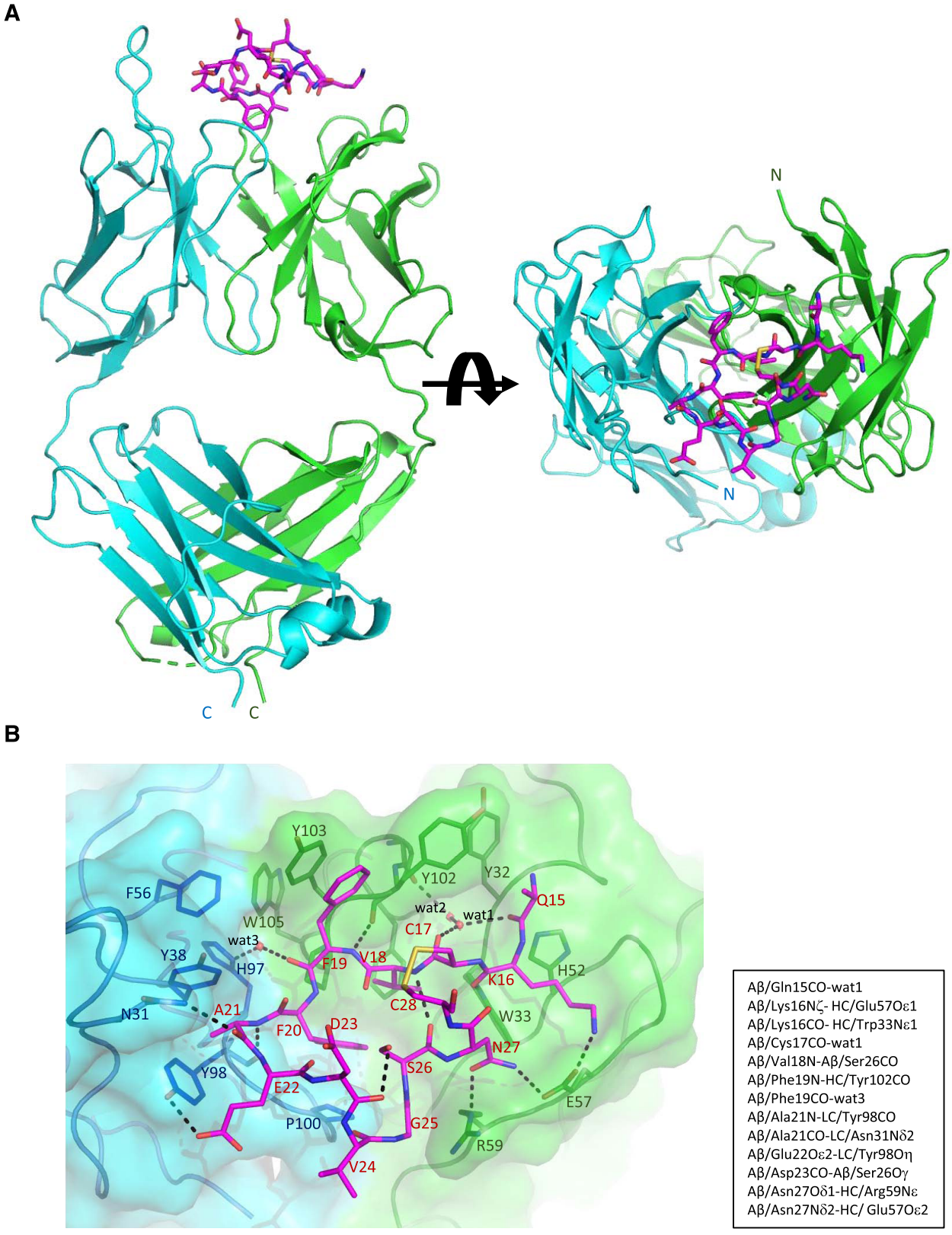

Figure 4. Crystal structure of TxCo-1 Fab in complex with SS-Aβ42 (15−30). (A) Front (left) and top (right) views of the crystal structure of TxCo-1 Fab in complex with the truncated form of SS-Aβ42 (15−30). Fab chains of H and L represented by ribbon models are indicated in green and cyan, and SS-Aβ42 (15−30) is represented by stick models in magenta. Dashed line shows the disorder (134−136 of H chain). (B) SS-Aβ42 (15−30) binding site in TxCo-1/SS-Aβ42 (15−30) complex. The chain color is the same as presented in (A). The predicted interactions are drawn with black dashed lines. The residue 15 of SS-Aβ42 (15−30) was truncated to alanine due to the poor electron density. Predicted interactions between TxCo-1 Fab and SS-Aβ42 (15−30) are summarized in the box chart.

https://doi.org/10.1021/acschemneuro.1c00416
ACS Chem. Neurosci. 2021, 12, 3418−3432

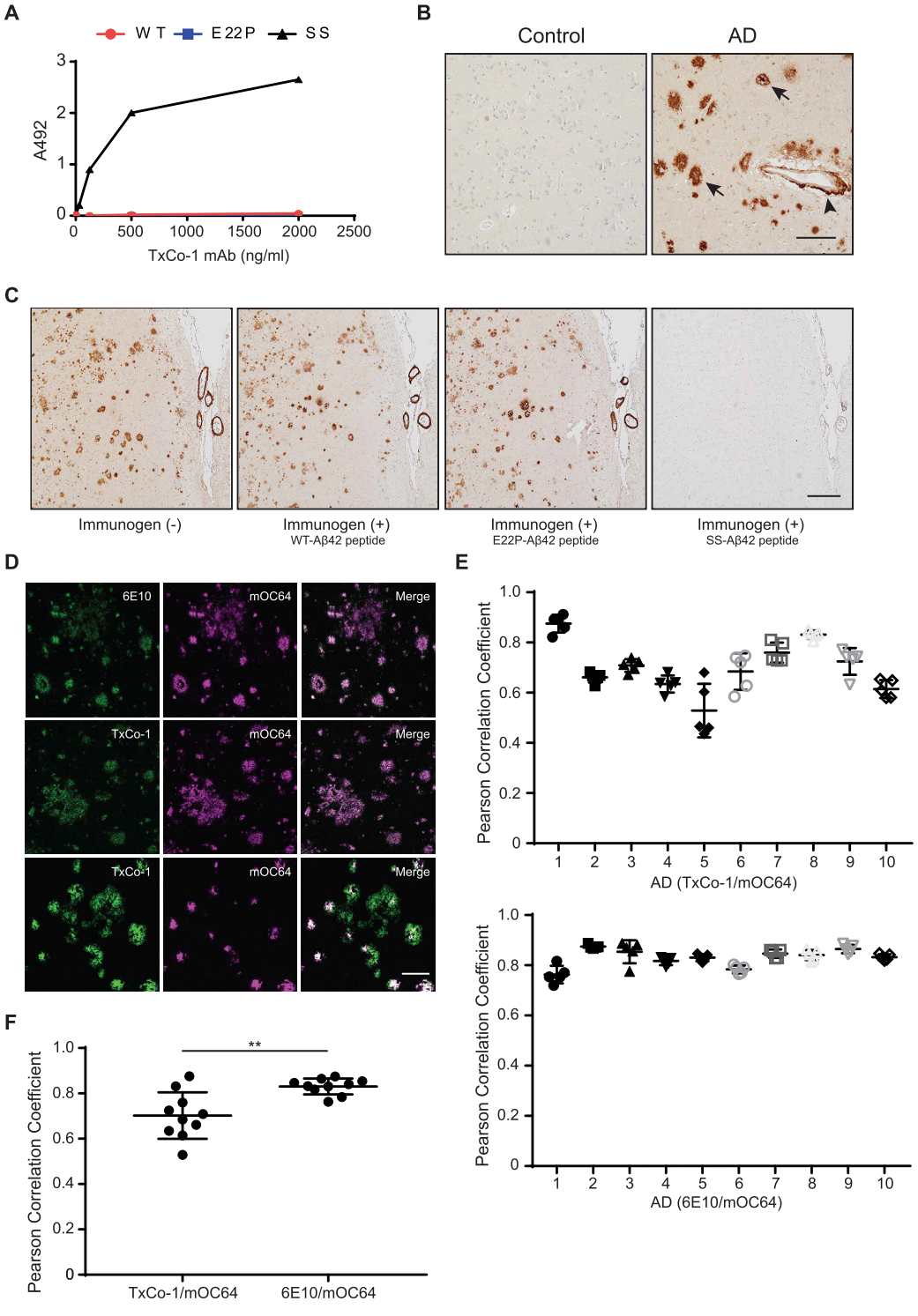

Figure 5. Characterization of immunoreactivity of TxCo-1 antibody on human brain sample. (A) Assessment of the binding affinity of TxCo-1 antibody against WT-Aβ42 (red), E22P-Aβ42 (purple), SS (black)-Aβ42 peptides by enzyme immunoassay. The TxCo-1 antibody exhibited high binding affinity to SS-Aβ42. (B) Representative images of postmortem human inferior parietal cortex of an age-matched non-neurological disease control subject and an Alzheimer's disease (AD) patient stained with TxCo-1 antibody. Senile plaques (arrow) and vascular amyloid (arrowhead) were identified by TxCo-1 antibody. The images were taken with 20× objective lens. Scale bar, 100 μm. (C) Specificity of TxCo-1 antibody on WT-Aβ42, E22P-Aβ42, SS-Aβ42. TxCo-1 antibody was incubated with or without Aβ peptides prior to incubation with brain tissues. Aβ peptides were in 20 molar excess to TxCo-1 antibody. The images were taken under 10× objective lens. Scale bar, 200 μm. (D) Representative images of postmortem human inferior parietal cortex sections of AD patients stained with TxCo-1, 6E10, and mOC64 antibodies. The images were taken with 40× objective lens. Scale bar, 50 μm. (E) Colocalization analysis of TxCo-1/mOC64 and 6E10/mOC64 signals in 10 AD cases. Pearson correlation coefficient (PCC) was calculated to reflect the degree of colocalization (0 = no colocalization, 1 = complete colocalization). (F) Comparison of PCC between AD samples stained with TxCo-1/mOC64 and 6E10/mOC64. Data information: Significance was calculated using Student's *t*-test: ** $P < 0.01$.

https://doi.org/10.1021/acschemneuro.1c00416
ACS Chem. Neurosci. 2021, 12, 3418−3432

with WT-Aβ42 and E22P-Aβ42 in 20 molar excess did not abolish TxCo-1 staining (Figure 5C). Lastly, we investigated the similarity of Aβ structures identified by the TxCo-1 antibody on human brain tissue with Aβ plaques stained with conventional Aβ antibodies: 6E10 and mOC64.[44] Double staining of brain tissues of AD patients with 6E10 and mOC64 showed extensive colocalization (Figure 5D, top panel). In contrast, double staining of TxCo-1 and mOC64 exhibited nonuniform patterns: extensive and moderate colocalization (Figure 5D, middle and bottom panels). The degree of colocalization, as Pearson correlation coefficient (PCC), of TxCo-1/mOC64 and 6E10/mOC64 in 10 AD cases showed that TxCo-1/mOC64 displayed a variety of PCC values ranging from 0.4 to 0.9, whereas 6E10/mOC64 displayed relatively uniform value (Figure 5E). The average of PCC values in each case was compared between TxCo-1/mOC64 and 6E10/mOC64 stained groups and showed statistical difference (Figure 5F). These data indicate that some Aβ structures stained with TxCo-1 antibody are different from Aβ plaques observed by using other Aβ antibodies.

Although genetic and experimental data suggest that excess Aβ is a primary etiological event in the development of AD, the fact that Aβ plaque burden does not correlate with clinical staging of AD has been a major question in the field.[2] As an explanation, it has been suggested that Aβ deposits as plaques could accumulate and sequester the soluble toxic Aβ aggregate.[45] When Aβ plaques lose their capacity as a buffer for binding Aβ, the toxic Aβ species could leak out with resulting damage in various areas in the brain. TxCo-1 antibody was developed using SS-Aβ42 as an immunogen, and a set of experiments supported its specificity to the immunogen.

In the crystal structure, the electron density of residues 16−28 of SS-Aβ42 (15−30) is clearly observed whereas both ends of SS-Aβ42 (15−30) must be disordered (Figure 4). Therefore, TxCo-1 antibody might recognize the residues 16−28 of SS-Aβ42 (15−30). TxCo-1 antibody was also specific to SS-Aβ42 and did not bind to WT-Aβ42 and E22P-Aβ42. From these results, it is appropriate to consider that the SS-Aβ42 would bind to TxCo-1 using the SS-Aβ42 (16−28) region of SS-Aβ42 in the same manner as that of SS-Aβ42 (15−30). These results imply the presence of naturally occurring Aβ with structural similarity to SS-Aβ42 in AD patient brains. Interestingly, the TxCo-1 immunoreactive pattern overlapped extensively but also had noticeable areas of no overlap with immunoreactivity identified with conventional Aβ antibodies. TxCo-1 immunoreactivity could suggest localization of Aβ oligomers in AD brain, and the pattern is consistent with soluble Aβ aggregates hypothesis. It will be of interest to investigate the patterns of TxCo-1 immunoreactivity with staging of AD pathology in a larger set of samples in a future study. The potential application for using TxCo-1 for measuring Aβ species in CSF and blood samples of AD patients also deserves consideration for future studies.

CONCLUSION

Pathophysiology of Aβ oligomers has been an area of significant research in AD. There remain unanswered questions due to the technical difficulty in studying the tertiary structures of Aβ oligomers with potent neurotoxicity. Furthermore, characterization of Aβ oligomers in human brain, i.e., their localization and dynamics in aging, has been quite challenging due to the lack of a suitable antibody that detects either a basic unit of toxic Aβ oligomers or toxic conformation of oligomers. The aim of this study was to establish biological tools to study "the conformation of toxic Aβ oligomers" using *in vitro* cell culture and human brain sections.

The results indicate that SS-Aβ could be a useful tool to model toxic Aβ oligomers. In addition, the antibody against SS-Aβ (TxCo-1) detected putative Aβ oligomers in AD brain with a different distribution compared with conventional Aβ antibody, 6E10, suggesting that TxCo-1 might be a useful tool for AD diagnosis in the early stage. However, several cautions should be made for SS-Aβ and TxCo-1 since SS-Aβ with an artificial disulfide bond is just a model of toxic Aβ in spite of the lack of the proline substitution at position 22.

The nucleation of Aβ could be affected by other factors like membrane, metal ions, and so on.[9] Specific interaction between GM1 and Aβ can result in the toxic Aβ species.[10,46] Sciacca et al. proposed a common molecular mechanism of membrane disruption by amylin, Aβ, and α-synuclein.[47] The role of apolipoproteins in the toxicity of Aβ oligomers has also been reported.[48] The effects on the toxic turn of Aβ at positions 22 and 23 and the resultant toxic oligomers by these factors remain to be investigated.

Although the mutation sites are concentrated in positions 22 and 23, there are other mutation sites (position 6, 7, or 21) in the Aβ of familial AD patients than positions 22 and 23. Therefore, this study does not exclude the existence of a toxic conformer with a turn other than at positions 22 and 23. For example, Sandberg's study reported the neurotoxicity of an S−S bridged Aβ at positions 21 and 30.[18]

In summary, this study demonstrated that the conformation-restricted Aβ via intramolecular disulfide bond at positions 17 and 28, which forms stable Aβ oligomers, has strong cytotoxicity *in vitro*. Furthermore, the TxCo-1 antibody, designed to detect Aβ with this toxic conformation of Aβ oligomers, identified this unique Aβ conformation in brain tissue of AD patients. These reagents, SS-Aβ42 and TxCo-1 antibody, should aid in understanding the pathological role of Aβ with toxic conformation in the development of AD.

MATERIALS AND METHODS

Human Postmortem Tissues. Autopsy-derived brain samples were provided by the Fukushimura Brain Bank (Aichi, Japan). All study subjects or their next of kin provided written informed consent for the brain donation. This study complies with the Declaration of Helsinki and was approved by the Ethics Committees of Shiga University of Medical Science (reference number R2018-101), Kyoto University (G0664-4), and Fukushimura Hospital (403). Formalin-fixed paraffin-embedded sections (5 μm thick) of inferior parietal cortex from ten patients with AD and three age-matched non-neurological disease control subjects were used in this study. The demographic details of subjects examined in this study are listed in Table 2 [age at death, sex, postmortem interval (PMI), causes of death and Braak stages for senile plaques/neurofibrillary tangle[49] in AD cases].

Antibodies. The primary antibodies used in this study were as follows: Aβ antibody 6E10 (803001, Biolegend, San Diego, CA, USA), Aβ antibody mOC64 (ab201060, Abcam, Cambridge, MA, USA), anti-β III tubulin (ab18207, Abcam, Cambridge, MA, USA), Iba1 (ab5076, Abcam, Cambridge, MA, USA), CD68 (ab213363, Abcam, Cambridge, MA, USA), TxCo-1 (this study).

Synthesis and Preparation of Aβ Peptides. WT-Aβ42, E22P-Aβ42, and SS-Aβ42 (hapten) were synthesized by previously reported methods.[29,39,50] The molecular weights were confirmed by ESI-qTOF-MS, and their purity was determined by HPLC (>98%) as reported previously.[29,39,51] 1,1,1,3,3,3-Hexafluoro-2-propanol (HFIP)

https://doi.org/10.1021/acschemneuro.1c00416
ACS Chem. Neurosci. 2021, 12, 3418−3432

Table 2. Summary of Sample Demography

case no.	age	sex	PMI (h)	Braak stage	NP diagnosis
1	84	F	3	C/5	AD
2	92	F	2	C/6	AD
3	92	F	5	C/5	AD
4	75	F	4.5	C/6	AD
5	88	F	1	C/6	AD
6	90	M	15	C/6	AD
7	83	F	3	C/6	AD
8	86	M	10.5	C/4	AD
9	98	F	2.5	C/5	AD
10	86	F	17	C/4	AD
11	86	M	16.5	0/1	non-AD
12	90	F	5.5	0/2	non-AD
13	82	M	16.5	0/1	non-AD

(FUJIFILM, Osaka, Japan) was used in the preparation of Aβ peptides for experiments. Synthesized Aβ peptides were dissolved in HFIP to a final concentration of 1 mM. The peptides were incubated for 60 min at 37 °C with mixing every 10 min, and HFIP was evaporated using water pump vacuum for 30 min at room temperature (RT). Dried peptides were dissolved in fresh dimethyl sulfoxide (DMSO) (Nacalai Tesque, Kyoto, Japan) to a final concentration of 400 μM. The peptides were stored at −80 °C until use.

ThioflavinT (Th-T) Binding Assay. Aβ peptides prepared at 400 μM were diluted to make final concentrations of 4 μM in phosphate buffered saline (PBS: 137 mM NaCl, 8.1 mM Na_2HPO_4, 2.68 mM KCl, 1.47 mM KH_2PO_4, pH 7.4) or RPMI1640 tissue culture media without phenol red (Nacalai Tesque, Kyoto, Japan) supplemented with 1% fetal bovine serum (FBS) in protein LoBind tubes (Eppendorf, Hamburg, Germany). For the control sample, DMSO was added either to PBS or 1% FBS/RPMI1640 and made its final concentration at 1%. For blank samples, PBS and 1% FBS/RPMI1640 were prepared. The samples were incubated at 37 °C for 24 h. Thioflavin T (Th-T) (Anaspec, Fremont, CA, USA) was dissolved in DMSO, adjusted to 10 mM. After 24 h incubation, 10 mM Th-T was diluted in the samples to make a final concentration of 20 μM. An amount of 100 μL of the samples was transferred to black 96-well nonbinding surface microplates (Greiner, Kremsmünster, Austria). The samples were incubated for 12 h at 24 °C. Th-T fluorescence was measured at RT using an Infinite M200 plate reader (Tecan, Männedorf, Switzerland) through the top of the plate with excitation filter of 430 nm and emission filter of 485 nm. The experiments were conducted in triplicate. Fluorescence intensity changes were calculated based on the fluorescence intensity of blank wells, as previously described.[52]

Nondenaturing PAGE. To observe Aβ aggregates under nondenaturing conditions (without detergents or reducing agents), we used a method based on the Blue-native PAGE (BN-PAGE) technique.[53] Aβ peptides prepared at 400 μM were diluted to make final concentrations of 0.25, 0.5, and 1.0 μM in either PBS or 1% FBS/RPMI1640 in protein LoBind tubes. The samples were incubated at 37 °C for 24 h. Then, 7.5 μL of each sample was mixed with 2.5 μL of NativePAGE 4× sample buffer (ThermoFisher, Waltham, MA, USA), and 2 μL of NativeMark unstained protein standard (ThermoFisher, Waltham, MA, USA) was loaded onto a NativePAGE 4−16%, Bis-Tris gel (ThermoFisher, Waltham, MA, USA) and electrophoresed for 25 min at 250 V using the dark-blue running buffer of the manufacturer. At that time, proteins had migrated through a third of the gel length, and then buffer was exchanged for light-blue running buffer. The gel was further electrophoresed at 150 V for 60 min, at 10 V for 70 min, then at 150 V until proteins reached about 1 cm above the bottom of the gel. After electrophoresis, proteins were transferred to PVDF membrane (Immobilon-P, Merck Millipore, Burlington, MA, USA) using a semidry transfer apparatus.[54] Membranes were blocked in 5% skimmed milk dissolved in Tris-buffered saline with 0.1% Tween 20 (TBST: 20 mM Tris-HCl, pH 7.6, 150 mM NaCl, 0.1% Tween 20) for 1 h at RT. Membranes were incubated with 6E10 antibody at 0.5 μg/mL in blocking buffer for 16 h at 4 °C. On the following day, membranes were washed for 10 min × 3 with TBST and incubated 1 h in HRP-labeled anti-mouse immunoglobulin G (IgG) (ThermoFisher, Waltham, MA, USA) at 1:5000 in 2% skimmed milk dissolved in TBST. Membranes were washed for 10 min × 3 with TBST and exposed to Chemi-Lumi One chemiluminescent substrate (Nacalai Tesque, Kyoto, Japan). The chemiluminescent signal was recorded with the Fusion Solo-S imager (Vilber, Marne-La-Vallée, France).

Photoinduced Cross-Linking of Unmodified Proteins (PICUP). Cross-linking of Aβ followed a published protocol.[30] Synthesized Aβ peptides were dissolved in HFIP to a final concentration of 1 mM. The peptides were incubated for 60 min at 37 °C with mixing every 10 min, and HFIP was evaporated using a water pump vacuum for 30 min at room temperature. Dried peptides were dissolved at a concentration of 50 μM in 10% (v/v) 60 mM NaOH and 90% (v/v) 10 mM phosphate buffer, pH 7.65. The samples were used immediately after being dissolved in the buffer or incubated at 37 °C for 5 min prior to the next step. Then, Aβ peptides were mixed with ammonium persulfate (Nacalai Tesque, Kyoto, Japan) and tris(2,2′-bipyridyl)dichlororuthenium(II) (TCI, Tokyo, Japan) in a molar ratio of 1:40:2. The mixture was irradiated for 0.25 s with 25000 lm LED flashlight, and the reaction was quenched with reducing tricine sample buffer [5% (v/v) β-mercaptoethanol, 3% (wt/vol) SDS, 10% glycerol (w/v), 0.05% Coomassie blue G-250 in 37.5 mM Tris/HCl (pH 7.0)]. Samples were separated by using 10−20% Tris-tricine gradient gel (ThermoFisher, Waltham, MA, USA). After SDS/PAGE, the bands were visualized by silver staining (silver stain II kit Wako, Osaka, Japan).

Morphological Analysis of Aβ Fibril in Confocal Microscope. Round cover glasses (C013001, Matsunami, Osaka, Japan) were placed in a 24-well cell culture plate (IWAKI, Shizuoka, Japan). Collagen I (Corning, Glendale, AZ, USA) (10 μg/mL in 0.02 M acetic acid) was added to the wells (500 μL/well) with the cover glasses and incubated at RT for 1 h. Treated wells were washed twice with PBS. Aβ peptides prepared at 400 μM were diluted to make final concentrations of 1.0 μM in either PBS or 1% FBS/RPMI1640 and transferred to the wells with the cover glasses. PBS or 1% FBS/RPMI1640 with Aβ peptides were incubated at 37 °C for 24 h. The cover glasses were transferred to a new 24-well plate and fixed with 50% acetone/50% EtOH for 15 min on ice. Once dried, the cover glasses were washed with PBS for 5 min × 2, blocked with 3% donkey serum in PBS containing 0.1% Tween 20 for 1 h at RT, and then incubated with 6E10 (1 μg/mL) in blocking buffer for 16 h at 4 °C. On the following day, the cover glasses were washed in PBS with 0.1% Tween 20 for 5 min × 3, then incubated with Alexa Fluor 488 anti-mouse IgG secondary antibody in PBS with 0.1% Tween 20 for 1 h at RT. The cover glasses were washed in PBS for 5 min × 3 and mounted on microscope slide using antifade mounting media (Vector Laboratories, Burlingame, CA, USA). Immunofluorescent images were taken on a Leica SP8 confocal microscope (Leitz, Wetzlar, Germany)

Morphological Analysis of Aβ Fibril by Atomic Force Microscopy (AFM). AFM images were obtained on a high-speed AFM (Nano Live Vision, RIBM, Tsukuba, Japan) using a silicon nitride cantilever (Olympus BL-AC10DS-A2). SS-Aβ42 peptides prepared at 400 μM were diluted to make a final concentration of 1.0 μM in PBS and incubated at 37 °C for 24 h. The samples (2 μL) at 0 and 24 h incubation were absorbed on a freshly cleaved mica plate for 5 min at RT and then washed with the buffer solution. Scanning was performed in the same buffer solution using a tapping mode.

THP-1 Cell Culturing and Differentiation. THP-1 monocytes (TIB-202) obtained from the American Type Culture Collection (Manassas, VA, USA) were cultured in suspension using RPMI1640 media supplemented with 10% FBS. Differentiation of cells was conducted by treatment with 100 nM phorbol myristate acetate (PMA) (Sigma-Aldrich, St. Louis, MO, USA) for 48 h in 5% FBS/RPMI1640. After 48 h, culture media with PMA were exchanged with

https://doi.org/10.1021/acschemneuro.1c00416
ACS Chem. Neurosci. 2021, 12, 3418−3432

fresh 5% FBS/RPMI1640 for 24 h. For differentiation in 96-well plate (IWAKI, Shizuoka, Japan), 25 000 cells were seeded in a well. For differentiation in 24-well plates on round cover glasses 100 000 cells were seeded in each well.

MTT Assay. Cell viability was assessed using MTT cell count kit (Nacalai Tesque, Kyoto, Japan) in accordance with the manufacturer's protocol. THP-1 cells were differentiated in 96-well plate as described above. Aβ peptides prepared at 400 μM were diluted to make final concentration of 25, 50, 100, 250, 500, and 1000 nM in RPMI1640 supplemented with 1% FBS. For the control sample, DMSO was mixed in 1% FBS/RPMI1640 and made its final concentration at 0.25%. 100 μL of prepared media containing Aβ peptides at various concentrations was added to differentiated THP-1 cells, and the cells were incubated at 37 °C for 24 h. 10 μL of MTT solution was added to each well, followed by 3 h incubation at 37 °C. 100 μL of MTT solubilization solution was applied on each well and mixed by pipetting. Absorbance at 570 nm was measured using an Infinite M200 plate reader. Cell viability was calculated based on the absorbance obtained by THP-1 cells incubated in 0.25% DMSO/1% FBS/RPMI1640 media as 100%. The experiments were conducted in triplicate, and the values were averaged.

Immunofluorescence Microscopy on THP-1 Cells. THP-1 cells were differentiated in 24-well plate as described above. Aβ peptides prepared at 400 μM were diluted to make final concentration of 0.25, 0.5, and 1.0 μM in 1% FBS/RPMI1640. 500 μL of prepared media containing Aβ peptides at various concentrations was applied on differentiated THP-1 cells, and the cells were incubated at 37 °C for 24 h. For experiments involving bafilomcyin A1 treatment,[40] 10 mM bafilomycin A1, dissolved in DMSO, was diluted to make final concentration of 50 μM in 1% FBS/RPMI1640. Then, Aβ peptides were diluted to make final concentrations of 0.25, 0.5, and 1.0 μM in 50 μM bafilomycin A1/1% FBS/RPMI1640. The cover glasses with differentiated THP1 cells were transferred to a new 24-well plate and fixed with 50% acetone/50% EtOH for 15 min on ice. Once dried, the cells were washed with PBS for 5 min × 2, blocked with 3% donkey serum in PBS containing 0.1% Tween 20 for 1 h at RT. Then, the cells were incubated with antibodies 6E10 (1 μg/mL), CD68 (1.2 μg/mL), and Iba1 (1 μg/mL) in blocking buffer for 16 h at 4 °C. On the following day, the cells were washed in PBS with 0.1% Tween 20 for 5 min × 3. The cells were incubated with Alexa Fluor 488 anti-mouse IgG, 555 anti-rabbit IgG, and 647 anti-goat IgG secondary antibodies in PBS with 0.1% Tween 20 for 1 h at RT. The cells were washed in PBS for 5 min × 3 and mounted on microscope slide using antifade mounting media. Immunofluorescent images were taken on a Leica SP8 confocal microscope.

Imaging and Data Analysis. Two montage images were captured for Aβ colocalization analysis on THP-1 cells. Each montage consisted of a 3 × 3 panel of images captured with a 40× objective lens encompassing an area of 0.762 mm^2. The pattern of 6E10 signal localized in THP1 cells was categorized into three groups: puncta, aggregate, and diffuse. The puncta and aggregate patterns were defined by 6E10-immunofluorescent spot less of 1 μm and over 3 μm, respectively. The diffuse pattern is defined by a 6E10-immunofluorescent diffuse signal throughout the cell body. THP-1 cells identified by Iba1 signal in the measured field were counted to calculate the fraction of the cells with 6E10 signal in each category. For the Aβ colocalization analysis on THP-1 cells treated with bafilomycin A1, the CD68 signal was used to calculate the fraction of the cells with 6E10 signal. The calculated values from the two montage images in each sample were averaged for the final analysis.

Development of TxCo-1 (10A1) Antibody. S−S bridged L17C, K28C-Aβ42 as an immunogen for the toxic conformation-restricted analog of Aβ42 was synthesized by a previously described method.[29] Mice (BDF-1, Charles River, Japan) were immunized weekly for a month with the immunogen (50 μg/mouse) mixed with complete Freund's adjuvant followed by booster injections with the antigen in incomplete Freund's adjuvant three times. A 96-well Maxisorp plate (Nunc, Roskilde, Denmark) coated with the immunogen (50 μg/mL) was incubated with the obtained clones for 1 h at RT, followed by treatment with a horseradish peroxidase-coupled anti-mouse IgG antibody [Immuno-Biological Laboratories (IBL), Gunma, Japan], and quantified using 3,3′,5,5′-tetramethylbenzidine (Kementec, Taastrup, Denmark) or *o*-phenylenediamine dihydrochloride substrate (Sigma-Aldrich, St. Louis, MO, USA). A total of 45 clones were obtained, identified for their ability to bind the immunogen, and then were subcloned to obtain seven clones. The screening was repeated to exclude weak or false positives. They were further screened for the inability to bind WT-Aβ42, E22P-Aβ42, and WT-Aβ40. As a result, clone 10A1 was selected, whose isotype was IgG1. Mice used for the development of antibodies were maintained according to the protocols approved by the Animal Care Committee of IBL Co., Ltd.

Crystallographic Study of the TxCo-1 Antibody. Fab fragment of the TxCo-1 antibody was prepared from papain digests and purified by gel filtration using Superdex 200 column (GE healthcare, Chicago, IL, USA) with PBS buffer. The purified Fab proteins were dialyzed against PBS, after absorption of Fc fragments with Protein A Sepharose, and concentrated to approximately 1 mg/mL to which a truncated hapten peptide [S−S bridged L17C, K28C-Aβ (15−30)] was added to adjust the molar ratio of the Fab and the peptide to 1:3. The mixture was further concentrated up to approximately 8 mg/mL using the Amicon centrifugation kit (Amicon Ultra 10K, 14 000*g*, 293 K, 7 min). The truncated hapten peptide was synthesized by the method reported previously,[29] and its molecular weight was confirmed by ESI-qTOF-MS. Crystallization condition was screened with the sitting-drop vapor diffusion method using commercial crystallization kits at 293 K. The crystals of TxCo-1-peptide complex were obtained from a 1:1 mixture of the protein and precipitant solution (18% (w/v) polyethylene glycol monomethyl ether 5000, and 0.2 M magnesium formate in 0.1 M sodium acetate buffer (pH 4.0)). The crystals belong to the space group *C*2 with cell dimensions of a = 185.0 Å, b = 40.5 Å, c = 69.4 Å, and β = 97.2°. Before data collection, crystals were soaked for 15−20 s in precipitant solutions containing 25% ethylene glycol as cryogenic solutions and then frozen in liquid N_2. X-ray diffraction data were collected under a nitrogen gas stream at 100 K using synchrotron radiation with an EIGER X4M detector on the BL1A beamline at Photon Factory. The diffraction data were processed and scaled with the XDS package[55] and Aimless program[56] from the CCP4 suite.[57] The structure of the TxCo-1-Fab complex was solved at 2.5 Å resolution by the molecular replacement method using the program Molrep[58] from the CCP4 suite,[57] with the coordinates of anti-E22P-Aβ antibody 24B3[59] as a search model (unpublished data). The models were manually constructed using the program Coot,[60] and structure refinement was performed with the program REFMAC.[57,61] The final model of TxCo-1-peptide consists of L-chain, H-chain, Aβ (residue numbers 15−28), 3 ethylene glycols, 2 polyethylene glycols, and 91 water molecules. The quality of the model was checked using the MolProbity[62] server at http://molprobity.biochem.duke.edu/. The data collection and refinement statistics are summarized in Table 1. Figures of crystal structure were prepared using the program PyMOL (The PyMOL Molecular Graphics System, version 2.3, Schrödinger, LLC.) unless otherwise stated.

PDB Reference. The atomic coordinates and structure factors of TxCo-1-peptide complex have been deposited in the Worldwide Protein Data Bank (wwPDB), with the accession code of 7E6P.

Enzyme Immunoassay (EIA). In a 96-well Maxisorp plate (Nunc, Roskilde, Denmark), each Aβ peptide (500 pmol/well) dissolved in 50 mM sodium carbonate was incubated for 2 h at RT, followed by blocking with 5% bovine serum albumin at 4 °C overnight, as previously described.[63] Briefly, after incubation of TxCo-1 antibody with each peptide for 1 h at RT, the plate was treated with a horseradish peroxidase-coupled anti-mouse IgG antibody (IBL, Gunma, Japan) and quantified using *o*-phenylenediamine dihydrochloride substrate (Sigma-Aldrich, St. Louis, MO, USA) before measurements at 492 nm with a microplate reader (MultiScan JX; Thermo Scientific).

Immunohistochemistry with Fluorescent Probes on Human Brain. Immunohistochemistry with fluorescent probes and screening of tissue quality of cerebellum with β-tubulin immunohistochemistry were performed as previously described.[64] High-quality samples were

https://doi.org/10.1021/acschemneuro.1c00416
ACS Chem. Neurosci. 2021, 12, 3418−3432

selected for this study. Tissue sections were deparaffinized in xylene and rehydrated in 100% EtOH for 5 min × 3, 90% EtOH for 5 min, and 70% EtOH for 5 min. After washing with tap water, samples were incubated with 70% formic acid for 12 min at RT prior to antigen retrieval. Antigen retrieval was performed in 1 mM EDTA (pH 8.0) by boiling for 10 min. For cerebellum, antigen retrieval was performed in citrate buffer (pH 6.0) (Abcam, Cambridge, MA, USA) by boiling for 10 min. Samples were blocked with 5% donkey serum in PBS containing 0.2% Triton X-100 for 1 h at RT. Then, samples were incubated with TxCo-1 (1 μg/mL)/mOC64 (1 μg/mL) or 6E10 (2 μg/mL)/mOC64 (1 μg/mL) in blocking buffer for 16 h at 4 °C. On the following day, samples were washed in PBS with 0.3% Triton X-100 for 5 min × 3. Then, samples were incubated with Alexa Fluor 488 anti-mouse IgG and 555 anti-rabbit IgG secondary antibodies in PBS with 0.5% Tween 20 for 1 h at RT. Samples were washed in PBS once for 5 min. For quenching lipofuscin autofluorescence, TrueBlack lipofuscin autofluorescence quencher (Biotium, Fremont, CA, USA) diluted 1/40 in 70% EtOH was applied to samples and incubated for 50 s at RT. Samples were washed with PBS for 5 min × 3 and coverslipped using antifade mounting media. Immunofluorescent images were taken on a Leica SP8 confocal microscope.

Immunohistochemistry with 3,3′-Diaminobenzidine (DAB) Development. Sections were deparaffinized in xylene for 5 min × 3 and rehydrated in 100%, 90%, and 70% EtOH. After washing with tap water, the tissues were incubated in 0.3% hydrogen peroxidase solution for 15 min at RT followed by 70% formic acid for 12 min at RT prior to antigen retrieval. After washing with tap water, antigen retrieval was performed in 1 mM EDTA (pH 8.0) by boiling for 10 min. Samples were blocked with 5% donkey serum in PBS containing 0.2% Triton X-100 for 1 h at RT. Samples were incubated with TxCo-1 antibody at 1 μg/mL in blocking buffer for 16 h at 4 °C. On the following day, samples were washed in PBS with 0.3% Triton-X100 for 5 min × 3, then biotinylated anti-mouse IgG (H+L) (Vector Laboratories, Burlingame, CA, USA) in PBS with 0.5% Tween 20 was applied and incubated for 1 h at RT. Samples were washed in PBS for 5 min x 3, and VECTASTAIN ABC-HRP Kit, Peroxidase (Vector Laboratories, Burlingame, CA, USA) was applied and incubated for 1 h at RT. Samples were washed in PBS for 5 min × 3, and DAB (Vector Laboratories, Burlingame, CA, USA) solution was applied and incubated for 2 min at RT. Counterstaining was performed with hematoxylin for 10 s. After dehydration and incubation in xylene, samples were coverslipped. Images were taken on Olympus BX50 light microscope.

Colocalization Analysis of mOC64 Antibody with 6E10 and TxCo-1 Antibodies. Brain tissues from 10 different AD cases were immunostained with TxCo-1/mOC64 or 6E10/mOC64 mixtures as described above. Five montage images were captured using a Leica SP8 confocal microscope for each case. The setting of the montages consisted of a 3 × 3 panel of images taken on ×40 objective lens encompassing an area of 0.762 mm^2. To quantify colocalization of TxCo-1 immunoreactivity (IR) with mOC64 IR and 6E10 IR with mOC64 IR, the images were analyzed using EzColocalization plugin for ImageJ.[65] The top 10% of pixels above threshold (FT 10%) were chosen for the analysis. The Pearson correlation coefficient was calculated to reflect the degree of colocalization (0 = no colocalization, 1 = complete colocalization).

Statistical Analysis. The data are presented as the mean ± SD. Statistical analyses were performed with GraphPad Prism (version 7.0). One-way analysis of variance with post-hoc Tukey's test for multiple comparisons was conducted for the data analysis in Figures 1A, 2A, and 3A,D. Two-way analysis of variance with post-hoc Tukey's test for multiple comparisons was conducted for the data analysis in Figure 3C,F. The Student's *t* test was conducted to the data analysis on Figure 4F. *p* values of <0.05 were considered significant.

AUTHOR INFORMATION

Corresponding Author

Ikuo Tooyama − *Molecular Neuroscience Research Center, Shiga University of Medical Science, Shiga 520-2192, Japan;* orcid.org/0000-0001-8054-9666; Phone: +81-77-548-2330; Email: kinchan@belle.shiga-med.ac.jp; Fax: +81-77-548-2331

Authors

Yusuke Kageyama − *Molecular Neuroscience Research Center, Shiga University of Medical Science, Shiga 520-2192, Japan*

Yumi Irie − *Division of Food Science & Biotechnology, Graduate School of Agriculture, Kyoto University, Kyoto 606-8502, Japan*

Yuka Matsushima − *Division of Food Science & Biotechnology, Graduate School of Agriculture, Kyoto University, Kyoto 606-8502, Japan*

Tatsuya Segawa − *Immuno-Biological Laboratories Co., Ltd., Fujioka, Gunma 375-0005, Japan*

Jean-Pierre Bellier − *Molecular Neuroscience Research Center, Shiga University of Medical Science, Shiga 520-2192, Japan*

Kumi Hidaka − *Department of Chemistry, Graduate School of Science, Kyoto University, Kyoto 606-8502, Japan*

Hiroshi Sugiyama − *Department of Chemistry, Graduate School of Science, Kyoto University, Kyoto 606-8502, Japan;* orcid.org/0000-0001-8923-5946

Daita Kaneda − *Choju Medical Institute, Fukushimura Hospital, Yamanaka, Aichi 441-8124, Japan*

Yoshio Hashizume − *Choju Medical Institute, Fukushimura Hospital, Yamanaka, Aichi 441-8124, Japan*

Hiroyasu Akatsu − *Choju Medical Institute, Fukushimura Hospital, Yamanaka, Aichi 441-8124, Japan; Department of Community-Based Medical Education, Nagoya City University Graduate School of Medicine, Nagoya, Aichi 467-8601, Japan*

Kunio Miki − *Department of Chemistry, Graduate School of Science, Kyoto University, Kyoto 606-8502, Japan;* orcid.org/0000-0002-8381-0871

Akiko Kita − *Institute for Integrated Radiation and Nuclear Science, Kyoto University, Sennan, Osaka 590-0494, Japan*

Douglas G. Walker − *Molecular Neuroscience Research Center, Shiga University of Medical Science, Shiga 520-2192, Japan*

Kazuhiro Irie − *Division of Food Science & Biotechnology, Graduate School of Agriculture, Kyoto University, Kyoto 606-8502, Japan;* orcid.org/0000-0001-7109-8568

Complete contact information is available at: https://pubs.acs.org/10.1021/acschemneuro.1c00416

Author Contributions

Y.K., D.G.W., and I.T designed the project and analyzed and interpreted experiments. Y.K., Y.I., Y.M., J.-P.B., and K.H. performed the experiments. T.S. developed TxCo-1 (10A1) antibody and prepared its Fab domain. H.S. supervised AFM imaging. D.K., Y.H., and H.A. performed brain autopsies and neuropathological examinations. K.I. supervised synthesis of Aβ peptides and EIA and provided the peptides. Y.I and K.I. synthesized the haptene peptide of TxCo-1 and prepared cocrystals of TxCo-1 and its haptene peptide for X-ray crystallography. A.K. and K.M. collected X-ray crystallographic data and determined the structure. Y.K. and I.T. drafted the manuscript. D.G.W. and K.I. reviewed the manuscript.

https://doi.org/10.1021/acschemneuro.1c00416
ACS Chem. Neurosci. 2021, 12, 3418−3432

Funding

This research was supported by JSPS KAKENHI Grant JP19H00921 to K.I. and I.T. and by JSPS KAKENHI Grant JP19K07843 to D.G.W.

Notes

The authors declare the following competing financial interest(s): Tatsuya Segawa is employed by Immuno-Biological Laboratories Co., Ltd. The remaining authors declare that the research was conducted in the absence of any commercial or financial relationships that could be construed as a potential conflict of interest.

■ ACKNOWLEDGMENTS

We are grateful to Takefumi Yamamoto at Central Research Laboratory of Shiga University of Medical Science and to Norihiro Ogawa at Choju Medical Institute for technical support. We thank the staff members at the beamlines of Photon Factory, SPring-8, and Paul Scherrer Institute (PSI) for their help with X-ray data collections with synchrotron radiation.

■ REFERENCES

(1) Hardy, J.; Selkoe, D. J. The amyloid hypothesis of Alzheimer's disease: progress and problems on the road to therapeutics. *Science* **2002**, *297*, 353−356.
(2) Selkoe, D. J.; Hardy, J. The amyloid hypothesis of Alzheimer's disease at 25 years. *EMBO Mol. Med.* **2016**, *8*, 595−608.
(3) Crouch, P. J.; Harding, S. M.; White, A. R.; Camakaris, J.; Bush, A. I.; Masters, C. L. Mechanisms of A beta mediated neurodegeneration in Alzheimer's disease. *Int. J. Biochem. Cell Biol.* **2008**, *40*, 181−198.
(4) Chen, G. F.; Xu, T. H.; Yan, Y.; Zhou, Y. R.; Jiang, Y.; Melcher, K.; Xu, H. E. Amyloid beta: structure, biology and structure-based therapeutic development. *Acta Pharmacol. Sin.* **2017**, *38*, 1205−1235.
(5) Almeida, Z. L.; Brito, R. M. M. Structure and Aggregation Mechanisms in Amyloids. *Molecules* **2020**, *25*, 1195.
(6) Fontana, I. C.; Zimmer, A. R.; Rocha, A. S.; Gosmann, G.; Souza, D. O.; Lourenco, M. V.; Ferreira, S. T.; Zimmer, E. R. Amyloid-β oligomers in cellular models of Alzheimer's disease. *J. Neurochem.* **2020**, *155*, 348−369.
(7) Lee, A. K.; Khaled, H.; Chofflet, N.; Takahashi, H. Synaptic Organizers in Alzheimer's Disease: A Classification Based on Amyloid-β Sensitivity. *Front. Cell. Neurosci.* **2020**, *14*, 281.
(8) Huang, Y. R.; Liu, R. T. The Toxicity and Polymorphism of β-Amyloid Oligomers. *Int. J. Mol. Sci.* **2020**, *21*, 4477.
(9) Nguyen, H. P.; Ramamoorthy, A.; Sahoo, R. B.; Zheng, J.; Faller, P.; Straub, E. J.; Dominguez, L.; Shea, E. J.; Dokholyan, V. N.; Simone, D. A.; et al. Amyloid oligomers: a joint experimental/computational perspective on Alzheimer's disease, Parkinson's disease, type II diabetes, and amyotrophic lateral sclerosis. *Chem. Rev.* **2021**, *121*, 2545−2647.
(10) Yanagisawa, K.; Odaka, A.; Suzuki, N.; Ihara, Y. GM1 ganglioside-bound amyloid β-protein (Aβ): a possible form of preamyloid in Alzheimer's disease. *Nat. Med.* **1995**, *1*, 1062−1066.
(11) Kotler, S. A.; Walsh, P.; Brender, J. R.; Ramamoorthy, A. Differences between amyloid-β aggregation in solution and on the membrane: insights into elucidation of the mechanistic details of Alzheimer's disease. *Chem. Soc. Rev.* **2014**, *43*, 6692−6700.
(12) Cheng, S. Y.; Cao, Y.; Rouzbehani, M.; Cheng, K. H. Coarse-grained MD simulations reveal beta-amyloid fibrils of various sizes bind to interfacial liquid-ordered and liquid-disordered regions in phase separated lipid rafts with diverse membrane-bound conformational states. *Biophys. Chem.* **2020**, *260*, 106355.
(13) Cerofolini, L.; Ravera, E.; Bologna, S.; Wiglenda, T.; Böddrich, A.; Purfürst, B.; Benilova, I.; Korsak, M.; Gallo, G.; Rizzo, D.; Gonnelli, L.; Fragai, M.; De Strooper, B.; Wanker, E. E.; Luchinat, C. Mixing Aβ (1-40) and Aβ (1-42) peptides generates unique amyloid fibrils. *Chem. Commun.* **2020**, *56*, 8830−8833.
(14) Nguyen, P. H.; Derreumaux, P. Structures of the intrinsically disordered Aβ, tau and α-synuclein proteins in aqueous solution from computer simulations. *Biophys. Chem.* **2020**, *264*, 106421.
(15) Bitan, G.; Lomakin, A.; Teplow, D. B. Amyloid beta-protein oligomerization: prenucleation interactions revealed by photo-induced cross-linking of unmodified proteins. *J. Biol. Chem.* **2001**, *276*, 35176−35184.
(16) Williams, T. L.; Serpell, L. C.; Urbanc, B. Stabilization of native amyloid β-protein oligomers by Copper and Hydrogen peroxide Induced Cross-linking of Unmodified Proteins (CHICUP). *Biochim. Biophys. Acta, Proteins Proteomics* **2016**, *1864*, 249−259.
(17) Cline, E. N.; Das, A.; Bicca, M. A.; Mohammad, S. N.; Schachner, L. F.; Kamel, J. M.; DiNunno, N.; Weng, A.; Paschall, J. D.; Bu, R. L.; Khan, F. M.; Rollins, M. G.; Ives, A. N.; Shekhawat, G.; Nunes-Tavares, N.; de Mello, F. G.; Compton, P. D.; Kelleher, N. L.; Klein, W. L. A novel crosslinking protocol stabilizes amyloid β oligomers capable of inducing Alzheimer's-associated pathologies. *J. Neurochem.* **2019**, *148*, 822−836.
(18) Sandberg, A.; Luheshi, L. M.; Söllvander, S.; Pereira de Barros, T.; Macao, B.; Knowles, T. P.; Biverstål, H.; Lendel, C.; Ekholm-Petterson, F.; Dubnovitsky, A.; Lannfelt, L.; Dobson, C. M.; Härd, T. Stabilization of neurotoxic Alzheimer amyloid-beta oligomers by protein engineering. *Proc. Natl. Acad. Sci. U. S. A.* **2010**, *107*, 15595−15600.
(19) Morimoto, A.; Irie, K.; Murakami, K.; Masuda, Y.; Ohigashi, H.; Nagao, M.; Fukuda, H.; Shimizu, T.; Shirasawa, T. Analysis of the secondary structure of beta-amyloid (Abeta42) fibrils by systematic proline replacement. *J. Biol. Chem.* **2004**, *279*, 52781−52788.
(20) Murakami, K.; Irie, K.; Ohigashi, H.; Hara, H.; Nagao, M.; Shimizu, T.; Shirasawa, T. Formation and Stabilization Model of the 42-mer Aβ Radical: Implications for the Long-Lasting Oxidative Stress in Alzheimer's Disease. *J. Am. Chem. Soc.* **2005**, *127*, 15168−15174.
(21) Murakami, K.; Hara, H.; Masuda, Y.; Ohigashi, H.; Irie, K. Distance measurement between Tyr10 and Met35 in amyloid beta by site-directed spin-labeling ESR spectroscopy: implications for the stronger neurotoxicity of Abeta42 than Abeta40. *ChemBioChem* **2007**, *8*, 2308−2314.
(22) Masuda, Y.; Uemura, S.; Ohashi, R.; Nakanishi, A.; Takegoshi, K.; Shimizu, T.; Shirasawa, T.; Irie, K. Identification of physiological and toxic conformations in Abeta42 aggregates. *ChemBioChem* **2009**, *10*, 287−295.
(23) Irie, K. New diagnostic method for Alzheimer's disease based on the toxic conformation theory of amyloid β. *Biosci., Biotechnol., Biochem.* **2020**, *84*, 1−16.
(24) Raskatov, J. A.; Teplow, D. B. Using chirality to probe the conformational dynamics and assembly of intrinsically disordered amyloid proteins. *Sci. Rep.* **2017**, *7*, 12433.
(25) Warner, C. J. A.; Dutta, S.; Foley, A. R.; Raskatov, J. A. Introduction of D-glutamate at a critical residue of Aβ42 stabilizes a prefibrillary aggregate with enhanced toxicity. *Chem.—Eur. J.* **2016**, *22*, 11967−11970.
(26) Foley, A.; Finn, T. S.; Kung, T.; Hatami, A.; Lee, H.-W.; Jia, M.; Rolandi, M.; Raskatov, J. A. Trapping and characterization of nontoxic Aβ42 aggregation intermediates. *ACS Chem. Neurosci.* **2019**, *10*, 3880−3887.
(27) Foley, A.; Raskatov, J. A. Understanding and controlling amyloid aggregation with chirality. *Curr. Opin. Chem. Biol.* **2021**, *64*, 1−9.
(28) Foley, A. R.; Lee, H. W.; Raskatov, J. A. A Focused Chiral Mutant Library of the Amyloid β 42 Central Electrostatic Cluster as a Tool To Stabilize Aggregation Intermediates. *J. Org. Chem.* **2020**, *85*, 1385−1391.
(29) Matsushima, Y.; Yanagita, R. C.; Irie, K. Control of the toxic conformation of amyloid β42 by intramolecular disulfide bond formation. *Chem. Commun.* **2020**, *56*, 4118−4121.

https://doi.org/10.1021/acschemneuro.1c00416
ACS Chem. Neurosci. 2021, 12, 3418−3432

(30) Bitan, G. Structural study of metastable amyloidogenic protein oligomers by photo-induced cross-linking of unmodified proteins. *Methods Enzymol.* **2006**, *413*, 217−36.
(31) Bohrmann, B.; Tjernberg, L.; Kuner, P.; Poli, S.; Levet-Trafit, B.; Näslund, J.; Richards, G.; Huber, W.; Döbeli, H.; Nordstedt, C. Endogenous proteins controlling amyloid beta-peptide polymerization. Possible implications for beta-amyloid formation in the central nervous system and in peripheral tissues. *J. Biol. Chem.* **1999**, *274*, 15990−15995.
(32) Reyes Barcelo, A. A.; Gonzalez-Velasquez, F. J.; Moss, M. A. Soluble aggregates of the amyloid-beta peptide are trapped by serum albumin to enhance amyloid-beta activation of endothelial cells. *J. Biol. Eng.* **2009**, *3*, 5.
(33) Jessen, N. A.; Munk, A. S.; Lundgaard, I.; Nedergaard, M. The Glymphatic System: A Beginner's Guide. *Neurochem. Res.* **2015**, *40*, 2583−2599.
(34) Tarasoff-Conway, J. M.; Carare, R. O.; Osorio, R. S.; Glodzik, L.; Butler, T.; Fieremans, E.; Axel, L.; Rusinek, H.; Nicholson, C.; Zlokovic, B. V.; Frangione, B.; Blennow, K.; Ménard, J.; Zetterberg, H.; Wisniewski, T.; de Leon, M. J. Clearance systems in the brain-implications for Alzheimer disease. *Nat. Rev. Neurol.* **2015**, *11*, 457−470.
(35) Tsuchiya, S.; Kobayashi, Y.; Goto, Y.; Okumura, H.; Nakae, S.; Konno, T.; Tada, K. Induction of maturation in cultured human monocytic leukemia cells by a phorbol diester. *Cancer. Res.* **1982**, *42*, 1530−1536.
(36) Klegeris, A.; Walker, D. G.; McGeer, P. L. Interaction of Alzheimer beta-amyloid peptide with the human monocytic cell line THP-1 results in a protein kinase C-dependent secretion of tumor necrosis factor-alpha. *Brain Res.* **1997**, *747*, 114−121.
(37) Sarlus, H.; Heneka, M. T. Microglia in Alzheimer's disease. *J. Clin. Invest.* **2017**, *127* (9), 3240−3249.
(38) Leng, F.; Edison, P. Neuroinflammation and microglial activation in Alzheimer disease: where do we go from here? *Nat. Rev. Neurol.* **2021**, *17* (3), 157−172.
(39) Morimoto, A.; Irie, K.; Murakami, K.; Ohigashi, H.; Shindo, M.; Nagao, M.; Shimizu, T.; Shirasawa, T. Aggregation and neurotoxicity of mutant amyloid beta (A beta) peptides with proline replacement: importance of turn formation at positions 22 and 23. *Biochem. Biophys. Res. Commun.* **2002**, *295*, 306−311.
(40) Klionsky, J. D.; Abdalla, C. F.; Abeliovich, H.; Abraham, T. R.; Acevedo-Arozena, A.; Adeli, K.; Agholme, L.; Agnello, M.; Agostinis, P.; Aguirre-Ghiso, A. J.; et al. Guidelines for the use and interpretation of assays for monitoring autophagy. *Autophagy* **2012**, *8*, 445−544.
(41) Cline, E. N.; Bicca, M. A.; Viola, K. L.; Klein, W. L. The Amyloid-β Oligomer Hypothesis: Beginning of the Third Decade. *J. Alzheimer's Dis.* **2018**, *64*, S567−S610.
(42) Yasumoto, T.; Takamura, Y.; Tsuji, M.; Watanabe-Nakayama, T.; Imamura, K.; Inoue, H.; Nakamura, S.; Inoue, T.; Kimura, A.; Yano, S.; Nishijo, H.; Kiuchi, Y.; Teplow, D. B.; Ono, K. High molecular weight amyloid β(1-42) oligomers induce neurotoxicity via plasma membrane damage. *FASEB J.* **2019**, *33*, 9220−9234.
(43) Irie, Y.; Murakami, K.; Hanaki, M.; Hanaki, Y.; Suzuki, T.; Monobe, Y.; Takai, T.; Akagi, K.-i.; Kawase, T.; Hirose, K.; Irie, K. Synthetic Models of Quasi-Stable Amyloid β40 Oligomers with Significant Neurotoxicity. *ACS Chem. Neurosci.* **2017**, *8*, 807−816.
(44) Kayed, R.; Head, E.; Sarsoza, F.; Saing, T.; Cotman, C. W.; Necula, M.; Margol, L.; Wu, J.; Breydo, L.; Thompson, J. L.; Rasool, S.; Gurlo, T.; Butler, P.; Glabe, C. G. Fibril specific, conformation dependent antibodies recognize a generic epitope common to amyloid fibrils and fibrillar oligomers that is absent in prefibrillar oligomers. *Mol. Neurodegener.* **2007**, *2*, 18.
(45) Brody, D. L.; Jiang, H.; Wildburger, N.; Esparza, T. J. Non-canonical soluble amyloid-beta aggregates and plaque buffering: controversies and future directions for target discovery in Alzheimer's disease. *Alzheimer's Res. Ther.* **2017**, *9*, 62.
(46) Hoshino, T.; Mahmood, M. I.; Mori, K.; Matsuzaki, K. Binding and aggregation mechanism of amyloid β-peptides onto the GM1 ganglioside-containing lipid membrane. *J. Phys. Chem. B* **2013**, *117*, 8085−94.
(47) Sciacca, M. F.; Lolicato, F.; Tempra, C.; Scollo, F.; Sahoo, B. R.; Watson, M. D.; Garcia-Viñuales, S.; Milardi, D.; Raudino, A.; Lee, J. C.; Ramamoorthy, A.; La Rosa, C. Lipid-chaperone hypothesis: a common molecular mechanism of membrane disruption by intrinsically disordered proteins. *ACS Chem. Neurosci.* **2020**, *11*, 4336−4350.
(48) Sahoo, B. R.; Bekier, M. E., II; Liu, Z.; Kocman, V.; Stoddard, A. K.; Anantharamaiah, G. M.; Nowick, J.; Fierke, C. A.; Wang, Y.; Ramamoorthy, A. Structural interaction of apolipoprotein A-I mimetic peptide with amyloid-β generates toxic hetero-oligomers. *J. Mol. Biol.* **2020**, *432*, 1020−1034.
(49) Braak, H.; Braak, E. Neuropathological stageing of Alzheimer-related changes. *Acta Neuropathol.* **1991**, *82*, 239−259.
(50) Irie, K.; Oie, K.; Nakahara, A.; Yanai, Y.; Ohigashi, H.; Wender, P. A.; Fukuda, H.; Konishi, H.; Kikkawa, U. Molecular Basis for Protein Kinase C Isozyme-Selective Binding: The Synthesis, Folding, and Phorbol Ester Binding of the Cysteine-Rich Domains of All Protein Kinase C Isozymes. *J. Am. Chem. Soc.* **1998**, *120*, 9159−9167.
(51) Fukuda, H.; Shimizu, T.; Nakajima, M.; Mori, H.; Shirasawa, T. Synthesis, aggregation, and neurotoxicity of the Alzheimer's Abeta1-42 amyloid peptide and its isoaspartyl isomers. *Bioorg. Med. Chem. Lett.* **1999**, *9*, 953−956.
(52) Xue, C.; Lin, T. Y.; Chang, D.; Guo, Z. Thioflavin T as an amyloid dye: fibril quantification, optimal concentration and effect on aggregation. *R. Soc. Open Sci.* **2017**, *4*, 160696.
(53) Schägger, H.; von Jagow, G. Blue native electrophoresis for isolation of membrane protein complexes in enzymatically active form. *Anal. Biochem.* **1991**, *199*, 223−231.
(54) Bellier, J. P.; Kimura, H. Acetylcholine synthesis by choline acetyltransferase of a peripheral type as demonstrated in adult rat dorsal root ganglion. *J. Neurochem.* **2007**, *101*, 1607−1618.
(55) Kabsch, W. XDS. *Acta Crystallogr., Sect. D: Biol. Crystallogr.* **2010**, *66*, 125−132.
(56) Evans, P. R.; Murshudov, G. N. How good are my data and what is the resolution? *Acta Crystallogr., Sect. D: Biol. Crystallogr.* **2013**, *69*, 1204−1214.
(57) Winn, M. D.; Ballard, C. C.; Cowtan, K. D.; Dodson, E. J.; Emsley, P.; Evans, P. R.; Keegan, R. M.; Krissinel, E. B.; Leslie, A. G. W.; McCoy, A.; McNicholas, S. J.; Murshudov, G. N.; Pannu, N. S.; Potterton, E. A.; Powell, H. R.; Read, R. J.; Vagin, A.; Wilson, K. S. Overview of the CCP4 suite and current developments. *Acta Crystallogr., Sect. D: Biol. Crystallogr.* **2011**, *67*, 235−242.
(58) Vagin, A.; Teplyakov, A. Molecular replacement with MOLREP. *Acta Crystallogr., Sect. D: Biol. Crystallogr.* **2010**, *66*, 22−25.
(59) Murakami, K.; Tokuda, M.; Suzuki, T.; Irie, Y.; Hanaki, M.; Izuo, N.; Monobe, Y.; Akagi, K.-i.; Ishii, R.; Tatebe, H.; Tokuda, T.; Maeda, M.; Kume, T.; Shimizu, T.; Irie, K. Monoclonal antibody with conformational specificity for a toxic conformer of amyloid β42 and its application toward the Alzheimer's disease diagnosis. *Sci. Rep.* **2016**, *6*, 29038.
(60) Emsley, P.; Cowtan, K. Coot: model-building tools for molecular graphics. *Acta Crystallogr., Sect. D: Biol. Crystallogr.* **2004**, *60*, 2126−2132.
(61) Kovalevskiy, O.; Nicholls, R. A.; Long, F.; Carlon, A.; Murshudov, G. N. Overview of refinement procedures within REFMAC5: utilizing data from different sources. *Acta Crystallogr. D. Biol. Crystallogr.* **2018**, *74*, 215−227.
(62) Chen, V. B.; Arendall, W. B., 3rd; Headd, J. J.; Keedy, D. A.; Immormino, R. M.; Kapral, G. J.; Murray, L. W.; Richardson, J. S.; Richardson, D. C. MolProbity: all-atom structure validation for macromolecular crystallography. *Acta Crystallogr., Sect. D: Biol. Crystallogr.* **2010**, *66*, 12−21.
(63) Murakami, K.; Horikoshi-Sakuraba, Y.; Murata, N.; Noda, Y.; Masuda, Y.; Kinoshita, N.; Hatsuta, H.; Murayama, S.; Shirasawa, T.; Shimizu, T.; Irie, K. Monoclonal antibody against the turn of the 42-residue amyloid β-protein at positions 22 and 23. *ACS Chem. Neurosci.* **2010**, *1*, 747−756.

https://doi.org/10.1021/acschemneuro.1c00416
ACS Chem. Neurosci. 2021, 12, 3418−3432

(64) Kageyama, Y.; Saito, A.; Pletnikova, O.; Rudow, G. L.; Irie, Y.; An, Y.; Murakami, K.; Irie, K.; Resnick, S. M.; Fowler, D. R.; Martin, L. J.; Troncoso, J. C. Amyloid β toxic conformer has dynamic localization in the human inferior parietal cortex in absence of amyloid plaques. *Sci. Rep.* **2018**, *8*, 16895.
(65) Stauffer, W.; Sheng, H.; Lim, H. N. EzColocalization: An ImageJ plugin for visualizing and measuring colocalization in cells and organisms. *Sci. Rep.* **2018**, *8*, 15764.

https://doi.org/10.1021/acschemneuro.1c00416
ACS Chem. Neurosci. 2021, 12, 3418−3432